Supporting Information

Conformational effects in the identification and quantification of ketohydroperoxides in the oxidation of n-pentane

Dongyang Li[1], Deshan Li[2], Olivier Herbinet[3], Jiabin Huang[1], Gustavo A. Garcia[4], Philippe Arnoux[3], Luc-Sy Tran[5], Guillaume Vanhove[5], Laurent Nahon[4], Majdi Hochlaf[6], Hans-Heinrich Carstensen[7,8], Frédérique Battin-Leclerc[3], Julien Bloino[2], Feng Zhang[1,9*], and Jérémy Bourgalais[3,*]

[1]Hefei National Laboratory for Physical Sciences at the Microscale, University of Science and Technology of China, Hefei, Anhui, 230026, People's Republic of China
[2]Scuola Normale Superiore, Pisa, Italy
[3]Université de Lorraine, CNRS, LRGP, F-54000 Nancy, France
[4]Synchrotron SOLEIL, L'Orme des Merisiers, Départementale 128, 91190 Saint-Aubin, France
[5]PC2A, Université de Lille, CNRS; Avenue Mendeleiev, 59650 Villeneuve-d'Ascq, France
[6]Université Gustave Eiffel, COSYS/IMSE, 5 Bd Descartes, 77454 Champs sur Marne, France
[7]Fundación Agencia Aragonesa para la Investigación y el Desarrollo (ARAID), Zagaroza, 50018, Spain
[8]Escuela de Ingeniería y Arquitectura, Universidad de Zaragoza, Zaragoza, 50018, Spain
[9]Hefei National Laboratory, University of Science and Technology of China, Hefei, Anhui 230088, People's Republic of China

Table of Content

I. Experimental Details for the Analysis of the JSR Gas Mixture and TPES Acquisition:

The JSR is housed into a high vacuum chamber with a pressure of approximately 10^{-4} mbar. At the outlet of the JSR, a micrometer pinhole is utilized to expand a gas sample. This expansion creates an effusive molecular beam, where reactive collisions are minimized due to the low number density and dilution with a carrier gas (He in this case). Consequently, reactive intermediates are preserved during the expansion and flow in a collision-free regime (no intermolecular interactions) to the ionization chamber.

Nevertheless, it is important to consider that a time delay exists between the exit of the JSR and the detection of molecules, which can lead to changes in concentrations inside the reactor and result in temporal profile shifts. Furthermore, as molecules have different energies, the time delay will have a distribution, leading to a blurring of the temporal profile.[1] In our study, we have mitigated these effects by: 1) positioning the reactor in close proximity to the ionization region (approximately 14 cm), and 2) adiabatically expanding the reactor contents to generate a supersonic beam. When helium is used as the dilutant or carrier gas, the time delay is less than 10 μs.

In the ionization chamber, the species present are subjected to direct ionization upon exposure to incident vacuum ultraviolet (VUV) photons. This process leads to the generation of electrons and ions. These particles subsequently travel in opposite directions, dispersing based on their respective kinetic energies, before reaching the velocity map imagers (VMI) and forming concentric rings. The arrival times of the dispersed particles are recorded, and by selecting the electron arrival time as the reference point for time-of-flight detection of the photoion, mass spectra can be plotted. With photoion-mass selection, the VMI system allows, by using an Abel inversion technique, the construction of a two-dimensional matrix of photoelectron spectra (PES) as a function of photon energy. By selecting a specific kinetic energy range, the corresponding threshold photoelectron spectrum (TPES) can be obtained.

II. Off-Line Measurements of KHPs in JSR Gas Mixture:

The sample was trapped at room temperature and then analyzed at LRGP in Nancy using gas chromatography (GC) coupled to both a quadrupole mass spectrometer (MS) and a flame ionization detector (FID). The collected sample was diluted in acetone and injected into the GC in the liquid state using an automatic liquid sampler and a split mode injector. Although a HP5 capillary column was used, a perfect peak separation could not be achieved and many species remained co-eluted. The outlet of the column was connected to an auxiliary pressure control device splitting the flow towards both detectors. The chromatogram obtained during the analysis of the sample collected at the outlet of the reactor at SOLEIL (the sample was collected during the entire campaign, ~5 days) is displayed in Figure S1. The GC analysis detected a large number of peaks corresponding to many species accumulated

during the 5 days. The MS displayed in Figure S2 corresponds to the peak at retention time 30.5 min in the chromatogram of Figure S1 and found to be similar to the one recorded by Hu et al.[2] and attributed to 2,4-KHP. This pattern is expected to resemble that reported by Jorand et al.[3] for 2-hexanone-4-hydroperoxide (see Figure S3) except for the fact that the KHP for n-pentane contains one CH_2 group less (-14 a.m.u.). More specifically, the following main fragments are expected for 2,4-KHP: m/z 43, 57, 71, 85, and 100.

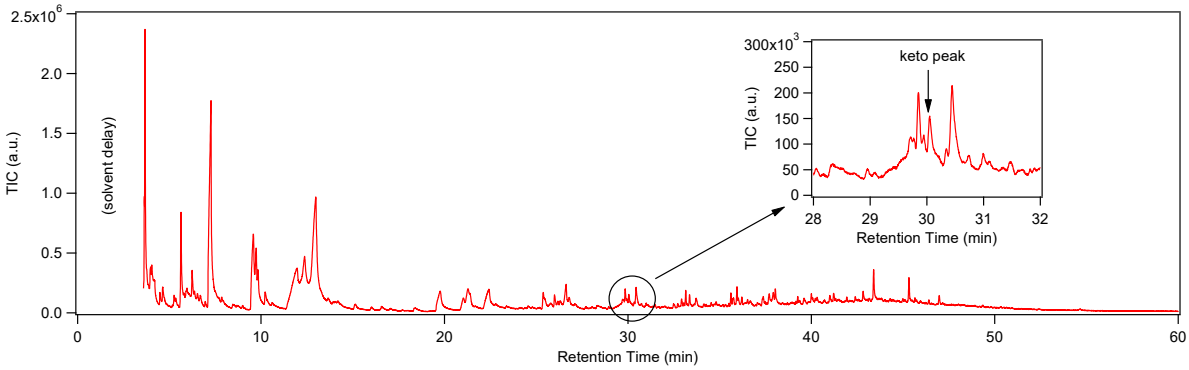

Figure S1: Chromatogram recorded during the analysis of the sample collected at the outlet of the reactor. TIC = total ion count.

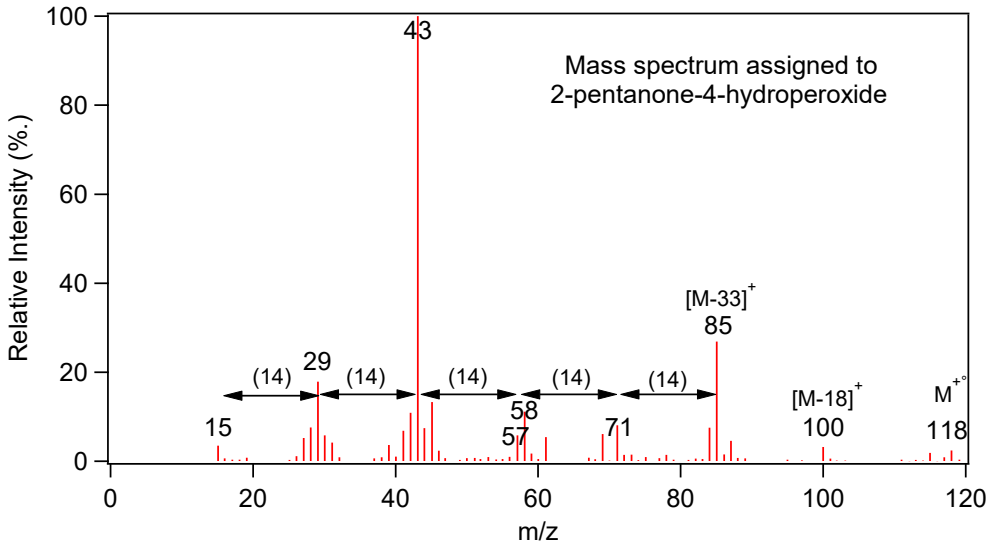

Figure S2. Mass spectrum from electronic ionization at 70 eV recorded during the analysis of the sample collected at the outlet of the JSR assigned to 2,4-KHP.

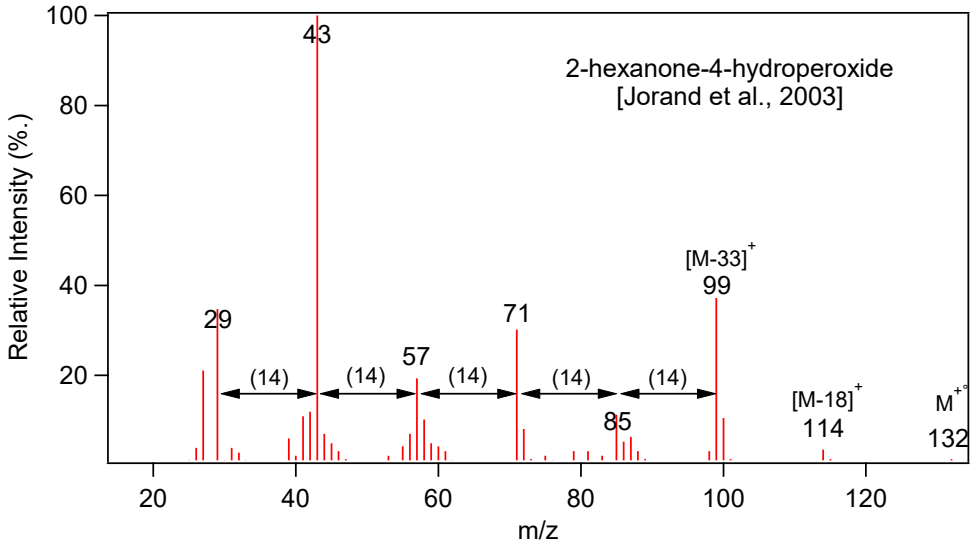

Figure S3. Mass spectrum recorded for 2-hexanone-4-hydroperoxide by Jorand et al.[3].

III. Ion Signals as Function of Temperature:

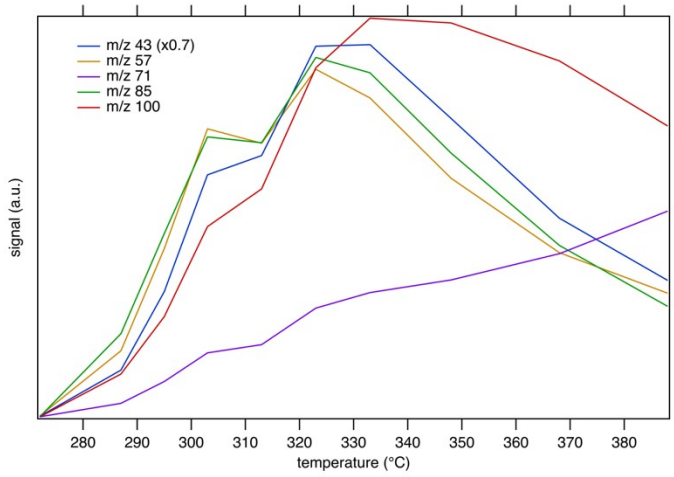

Figure S4. Ion signal at 10.5eV as a function of temperature for m/z 43, 57, 71, 85, and 100 (numbers in the graphs indicate factors by which the signals are multiplied/divided).

IV. Theoretical Method:

With numerous publications focusing on testing the performance of theoretical methods,[4] DFT offers an excellent compromise between required computation time and the quality of the results, while CCSD(T) calculations provide benchmark-quality results, making the combination of DFT and CCSD(T) as universal choice for most of system. In terms of basis selection, the more functions included in the basis set, the better the accuracy, albeit at a higher computational cost. Due to the influence of weak interactions, diffuse functions are necessary for achieving higher accuracy on energies.

For the conformational analysis, molecular dynamics simulations were initially performed at 585 K using Molclus[5] and xtb[6]. The structure was sampled every 50 femtoseconds, with a total sampling

time of 100 picoseconds resulting in 2,000 conformers. Subsequently, these conformers underwent optimization and screening using the gfn0-xtb[7], gfn2-xtb[6], and M06-2X-D3/cc-pVTZ[8–10] methods sequentially. The screening criteria considered conformers with an energy difference less than 0.5 kcal/mol and a root mean square displacement (RMSD) less than 0.5 Å to be identical. Single-point energies were calculated using CCSD(T)/aug-cc-pVTZ[10,11], and the zero-point energy from M06-2X-D3/cc-pVTZ was corrected by a factor of 0.971. Finally, Gibbs free energies at 585 K were obtained using the Shermo program[12] to generate the Boltzmann distribution.

The structures of dehydration and OOH dissociation mechanism were optimized by M06-2X-D3/cc-pVTZ method. Additionally, frequency calculations and intrinsic reaction coordinates (IRCs) were performed using the same method, with a zero-point energy (ZPE) correction factor of 0.971[13]. To enhance accuracy, high-level single-point energies were further refined using CCSD(T)/aug-cc-pVTZ. All density functional theory (DFT) calculations were carried out using the Gaussian 16 program[14], while coupled-cluster calculations were conducted using the ORCA program package[15].

Table S1. Energies(relative to Conf-1), Boltzmann distribution at 585K, adiabatic ionized energies (AIE) and vertical ionized energies (VIE) of the main 2,4-KHP conformers considered in this work, calculated at the (R)CCSD(T)/aug-cc-pVTZ//M06-2X-D3/cc-pVTZ level of theory

	Energies/eV	Boltzmann distribution	AIE/eV	VIE/eV
Conf-1	0.000	26.00%	9.508	9.963
Conf-2	0.045	26.03%	9.034	9.749
Conf-3	0.019	13.74%	9.062	10.239
Conf-4	0.065	22.50%	9.276	9.814
Conf-5	0.085	11.05%	9.317	9.513
Conf-6	0.211	0.72%	9.340	9.548

Table S2. Optimized coordinates (in Å) and frequencies (in cm^{-1}) of the 2,4-KHP conformers considered in this work and their cations, calculated by M06-2X-D3/cc-pVTZ

Neutral 2,4-KHP Conformers		
	Geometry/angstrom	Frequencies/cm^{-1}
Conf-1	C 2.471463 -0.816506 0.466211 C 1.435742 0.006717 -0.247307 C 0.193173 -0.705265 -0.734401 C -0.911806 -0.642701 0.333730 C -2.250466 -1.092273 -0.219456 O 1.564323 1.199413 -0.401674 O -0.986798 0.647010 0.920240 O -1.241962 1.597288 -0.105256 H 3.246642 -0.175716 0.874573 H 1.998172 -1.393206 1.263047 H 2.907632 -1.533642 -0.231588 H 0.402471 -1.751048 -0.960457 H -0.157930 -0.208015 -1.637542	48.0156 118.5248 140.7308 182.8299 208.6158 224.4166 283.7271 321.0880 417.3149 444.5435 535.9398 569.4504 605.2617 624.6246 818.0307 843.5070 907.6400 958.8217 972.2566 1001.7593 1037.5625 1109.4832 1137.9102 1162.4765 1212.4704 1268.6026 1315.8637 1359.9427 1380.3642 1395.0212 1408.7874 1462.9945 1473.6313 1476.7841 1483.3901 1490.5300 1506.1058 1832.9643 3063.5262

	H -0.629101 -1.263389 1.188295 H -2.565344 -0.415624 -1.011873 H -3.001591 -1.082006 0.568101 H -2.178061 -2.101359 -0.625274 H -0.336024 1.874483 -0.326416	3067.3237 3073.7039 3090.1212 3125.8158 3145.7748 3149.8122 3161.6814 3185.9238 3692.5977
Conf-2	C -2.915081 0.143304 -0.520434 C -1.605684 -0.085674 0.188329 C -0.509534 0.929329 -0.088344 C 0.866993 0.415121 0.277420 C 1.943580 1.480016 0.236873 O -1.436998 -1.012087 0.939266 O 1.116590 -0.600699 -0.691177 O 2.204153 -1.386073 -0.234092 H -3.678503 -0.516535 -0.119486 H -3.223653 1.185525 -0.430493 H -2.776936 -0.060670 -1.584055 H -0.738743 1.828628 0.490762 H -0.534935 1.223622 -1.140495 H 0.819621 -0.057868 1.260514 H 2.917650 1.024297 0.402763 H 1.773182 2.228261 1.011232 H 1.950466 1.974207 -0.735102 H 1.740245 -2.131164 0.169322	40.3632 64.5598 114.4099 139.7134 192.9236 242.1739 284.4168 317.8033 336.0729 353.6156 464.6424 486.8489 531.6802 630.0906 805.5358 842.9529 888.2613 956.9828 976.3596 997.6327 1061.2530 1133.0196 1140.6823 1173.9632 1199.4426 1262.4538 1324.8734 1379.0066 1388.2678 1408.7225 1417.6354 1424.0100 1444.2752 1467.8863 1479.4848 1489.6348 1506.9401 1853.9341 3061.1705 3065.8172 3066.8980 3081.3558 3104.6843 3129.5303 3139.4697 3157.6895 3182.8153 3810.9595
Conf-3	C -2.491032 0.390842 -0.211073 C -1.252154 -0.403393 0.097365 C -0.259050 0.182760 1.078208 C 1.007263 0.710264 0.376158 C 0.772315 1.979053 -0.421302 O -1.047320 -1.481187 -0.413070 O 1.511345 -0.211245 -0.569662 O 1.733676 -1.455949 0.072072 H -2.221330 1.409681 -0.493299 H -3.059718 -0.088035 -1.002357 H -3.099662 0.463999 0.692723 H 0.031784 -0.611163 1.764171 H -0.703581 0.996119 1.651659 H 1.763069 0.881022 1.148342 H 0.059025 1.797557 -1.225683 H 1.705530 2.314901 -0.868862 H 0.388676 2.768177 0.224058 H 0.890546 -1.902369 -0.121607	66.1815 111.4520 155.0972 195.9605 220.2390 245.4670 273.1971 338.2935 404.3967 476.4753 514.3405 537.2927 605.6712 668.5257 788.5531 853.4271 907.4230 940.2618 985.6201 1019.5837 1056.1779 1092.8421 1121.5614 1200.8638 1210.6597 1273.4997 1304.2503 1368.4114 1387.7548 1406.6888 1419.2915 1464.5202 1474.0170 1476.8912 1482.5824 1492.0292 1509.5451 1829.3195 3049.9231 3063.3908 3071.8410 3093.6043 3126.2363 3145.2243 3147.2522 3157.4160 3184.1427 3686.9112
Conf-4	C 3.038079 -0.626190 0.270519 C 1.755009 0.026912 -0.178543 C 0.477776 -0.684585 0.215584 C -0.779298 0.095318 -0.121027 C -0.978635 1.309936 0.763389 O 1.749518 1.048626 -0.817738 O -1.824427 -0.860136 0.052517 O -3.017108 -0.301550 -0.478751 H 3.887043 -0.119357 -0.178081 H 3.109141 -0.567303 1.358101 H 3.042527 -1.683619 0.004898 H 0.513398 -0.921786 1.282743 H 0.461434 -1.645478 -0.307001 H -0.752408 0.392717 -1.171024 H -0.156253 2.009107 0.624996 H -1.020379 1.006915 1.811397 H -1.904121 1.820996 0.504531 H -3.521838 -0.116051 0.321688	50.7819 80.6869 109.9725 136.5816 161.3496 221.5602 266.0083 298.0248 335.1258 342.3812 462.0892 490.0147 534.2612 616.8740 819.9870 853.7866 888.2797 953.5845 973.2383 993.9931 1051.4658 1137.4089 1138.2612 1172.4962 1201.2078 1254.0013 1324.7194 1380.3253 1387.9492 1399.7136 1408.8054 1420.5767 1454.7179 1469.6785 1480.5543 1494.9777 1510.1782 1849.1979 3057.1568 3063.3363 3069.1730 3084.6508 3099.3029 3134.0804 3143.0857 3160.6547 3183.6978 3836.8643
Conf-	C -1.779984 -0.953264 0.975026	61.3265 88.5346 112.9831

5	C -1.693081 0.131253 -0.068774 C -0.496307 1.067535 -0.012138 C 0.817710 0.390874 0.338455 C 1.994121 1.346137 0.306672 O -2.544494 0.281369 -0.906237 O 0.950420 -0.639847 -0.636409 O 1.994239 -1.504248 -0.206718 H -0.987462 -1.682597 0.798667 H -1.631705 -0.540107 1.974139 H -2.748490 -1.439424 0.909770 H -0.705514 1.824208 0.749422 H -0.424999 1.574565 -0.974086 H 0.749409 -0.087774 1.319614 H 2.066982 1.816702 -0.674313 H 2.920578 0.815825 0.518386 H 1.869930 2.126177 1.057499 H 2.635201 -1.400976 -0.919621	187.9402 199.1766 212.1539 247.7535 291.1584 320.1570 403.3598 461.8444 477.3529 557.7937 588.6374 797.8404 822.4325 896.6968 956.3257 986.5428 1007.8945 1060.6179 1126.4987 1136.1109 1169.3086 1237.5625 1267.7218 1306.9876 1378.3354 1389.9450 1392.9265 1409.6681 1415.7293 1452.3693 1471.7328 1483.6598 1490.7022 1506.8857 1856.0612 3059.7207 3064.6857 3067.1973 3069.2684 3130.6809 3131.3486 3142.8724 3154.8325 3183.6801 3841.3657
Conf-6	C -1.619657 0.670781 -1.217651 C -1.616054 -0.124667 0.062714 C -0.578928 0.195604 1.133946 C 0.880026 0.248984 0.673742 C 1.332216 1.566776 0.070542 O -2.434950 -0.983234 0.268543 O 1.000929 -0.826078 -0.254157 O 2.379192 -0.988266 -0.558729 H -1.586357 1.740832 -1.010061 H -0.732835 0.414301 -1.798282 H -2.512957 0.425315 -1.784436 H -0.703344 -0.564334 1.901911 H -0.836270 1.164871 1.569735 H 1.515883 0.023025 1.534577 H 1.264910 2.356275 0.819275 H 0.725092 1.847465 -0.787135 H 2.367924 1.485901 -0.251833 H 2.550967 -1.857888 -0.178775	58.1236 92.6873 124.4413 197.7895 202.3147 227.5142 262.4311 298.4026 327.1169 383.0796 466.6080 479.9096 545.8571 657.1426 767.5044 855.5207 871.3688 970.3230 987.8262 1009.4887 1059.3065 1103.3526 1133.8891 1166.9229 1224.6483 1286.1551 1334.7163 1373.4939 1387.7776 1393.2881 1408.7314 1425.0177 1461.8414 1475.6863 1481.4136 1496.2114 1511.6417 1849.8624 3050.6142 3069.3085 3072.0215 3081.6188 3141.1390 3145.1322 3153.3592 3173.3503 3180.9115 3834.6416

Cationic 2,4-KHP Conformers

	Geometry/angstrom	Frequencies/cm^{-1}
Conf-1^{+}	C 2.683166 -0.714684 0.254395 C 1.392390 -0.072029 -0.140365 C 0.171938 -0.937273 -0.405192 C -1.074260 -0.613603 0.434103 C -2.359552 -0.991565 -0.259599 O 1.338668 1.132037 -0.289082 O -1.065705 0.791047 0.796144 O -0.835428 1.499450 -0.348346 H 3.472300 0.019902 0.371252 H 2.515032 -1.261680 1.184956 H 2.941049 -1.446325 -0.514610 H 0.438355 -1.980147 -0.252361 H -0.053205 -0.784208 -1.463739 H -0.999483 -1.074335 1.418250 H -2.465461 -0.445374 -1.196443 H -3.212721 -0.777846 0.380391 H -2.351069 -2.058846 -0.479965 H -0.667166 2.403505 -0.017500	75.2112 96.7376 166.7418 222.7888 240.6728 263.7193 311.8752 320.4744 374.2015 435.8139 500.0478 532.0296 580.9992 651.6447 785.1651 823.1380 868.9597 908.6832 941.2652 1000.8025 1007.6067 1060.6192 1136.0360 1144.3869 1187.1049 1258.2520 1317.6224 1362.8739 1363.9301 1372.8624 1422.9986 1433.4100 1448.1694 1460.9082 1464.9309 1487.5227 1498.7152 1705.0529 3058.5207 3074.4931 3075.8268 3123.9807 3126.2910 3152.9928 3161.3114 3168.2328 3203.0100 3682.1035
Conf-2^{+}	C -2.972634 0.199522 0.099257 C -1.512858 -0.100356 -0.024558 C -0.520525 1.046519 -0.131436 C 0.844299 0.563648 0.307699 C 1.979908 1.518464 -0.026818	80.8860 114.6891 131.8672 159.9156 215.8770 236.5161 322.0381 340.7100 370.2942 398.9062 454.8807 477.2560 529.3297 638.4333 789.5409

	O -1.082190 -1.228836 -0.056867 O 1.046432 -0.662808 -0.435473 O 1.876368 -1.467626 0.271895 H -3.560056 -0.706787 0.000370 H -3.140522 0.653771 1.078296 H -3.251903 0.935065 -0.655979 H -0.839547 1.900622 0.464025 H -0.515828 1.362008 -1.179528 H 0.852186 0.281481 1.360478 H 2.929315 1.082013 0.274478 H 1.828029 2.443122 0.527787 H 1.997825 1.741002 -1.092052 H 2.066470 -2.184925 -0.359183	830.6247 885.3684 933.3501 968.0705 993.7630 1001.5900 1057.9566 1125.2026 1147.8513 1194.2672 1238.6083 1313.5817 1349.4816 1378.5877 1384.3822 1407.7207 1446.0621 1454.5024 1470.2662 1481.1928 1496.9836 1498.4098 1754.3911 3065.8943 3069.6424 3080.6581 3117.5470 3135.2794 3145.5482 3165.6359 3175.6477 3202.6904 3725.7323
Conf-3^{+}	C -2.743221 0.014292 0.094496 C -1.257791 -0.073715 -0.102548 C -0.343166 0.406390 1.012409 C 1.059811 0.583790 0.444328 C 1.244413 1.803015 -0.427696 O -0.773372 -0.530271 -1.108375 O 1.358863 -0.548479 -0.389186 O 1.322630 -1.682183 0.378683 H -3.017498 1.070601 0.048943 H -3.262644 -0.541096 -0.678638 H -2.996603 -0.353681 1.088324 H -0.384781 -0.357341 1.793126 H -0.719714 1.333464 1.443940 H 1.787952 0.546314 1.259774 H 0.520882 1.821407 -1.241168 H 2.247185 1.822628 -0.847477 H 1.112235 2.692790 0.185320 H 1.687731 -2.350251 -0.227051	79.5243 115.3069 153.6179 181.5553 204.5337 248.3806 301.3830 333.5822 375.5823 383.5561 464.4213 511.1470 535.5392 675.5925 795.4826 823.6603 866.7349 913.5711 958.2443 990.6686 1001.8401 1041.6561 1122.7128 1162.9545 1171.7417 1231.3500 1279.2381 1325.1543 1346.8611 1374.0012 1425.8787 1443.4175 1454.0208 1471.3821 1484.1359 1487.4276 1504.3253 1735.1047 3067.6414 3069.2432 3085.1829 3085.4502 3139.7954 3144.4869 3165.2143 3173.4219 3204.5838 3741.4725
Conf-4^{+}	C 2.949077 -0.651330 0.491418 C 1.747224 -0.011160 -0.143771 C 0.402171 -0.727715 0.112405 C -0.713031 0.250932 -0.281116 C -1.019579 1.332561 0.710850 O 1.775572 0.972834 -0.821251 O -1.827796 -0.618897 -0.574050 O -2.872977 -0.412564 0.215674 H 3.850653 -0.187500 0.104211 H 2.890819 -0.506781 1.571825 H 2.950835 -1.724417 0.301612 H 0.304060 -1.051730 1.148875 H 0.401171 -1.614846 -0.525736 H -0.446936 0.647033 -1.272767 H -0.132244 1.958754 0.782047 H -1.249671 0.923278 1.693614 H -1.847538 1.955235 0.376717 H -3.514701 -1.089743 -0.082100	48.5153 75.1381 105.7067 117.8793 198.2441 276.5432 301.4164 329.4723 337.7564 425.2360 482.3801 552.5338 575.2574 621.0376 720.9721 810.2244 825.2115 871.4489 966.1286 994.5812 1043.1522 1060.0861 1126.6538 1154.1146 1169.3224 1211.5427 1272.8577 1284.2176 1338.6445 1382.3777 1425.7360 1452.9288 1460.9287 1470.2976 1484.0253 1489.0612 1496.1879 1850.3842 2996.3502 3070.5156 3077.9275 3079.2999 3135.9490 3142.4266 3160.7758 3169.4458 3195.4862 3653.7780
Conf-5^{+}	C -1.796328 -0.838943 1.023303 C -1.581553 0.207727 -0.055129 C -0.389920 1.216003 0.049679 C 0.858187 0.391853 0.340227 C 2.106314 1.249336 0.232320 O -2.293113 0.306547 -0.999625 O 0.804360 -0.635831 -0.635730 O 1.615992 -1.693594 -0.154762 H -1.012909 -1.583187 0.857246 H -1.655774 -0.354055 1.987816 H -2.783015 -1.276913 0.919378	59.6330 70.5272 117.4588 171.0961 189.3821 217.1721 249.6510 282.4504 303.9759 335.9707 404.8802 455.0300 489.5313 558.6070 662.0437 834.7465 880.5322 906.7094 931.9708 979.5227 1023.7953 1073.2905 1090.0366 1116.7365 1142.8202 1202.8540 1267.5887 1324.7430 1351.3710 1387.7491 1399.2579 1424.7220 1444.3520

	H -0.652192 1.894178 0.864333 H -0.328678 1.754231 -0.892642 H 0.793795 -0.068272 1.328828 H 2.178151 1.700437 -0.755936 H 2.970459 0.606938 0.397466 H 2.110921 2.030648 0.990531 H 2.181122 -1.876828 -0.918492	1446.3517 1461.8104 1485.2506 1489.7692 1695.5987 3061.0338 3073.3776 3083.4103 3091.8746 3153.7296 3156.0362 3164.1936 3177.1042 3212.0159 3809.0901
Conf-6^+	C -1.644264 0.549919 -1.296554 C -1.514103 -0.080158 0.079055 C -0.561039 0.473684 1.173514 C 0.890471 0.352548 0.667338 C 1.389609 1.531376 -0.137907 O -2.171547 -1.028904 0.376092 O 0.854868 -0.864397 -0.066253 O 2.156028 -1.124595 -0.552965 H -1.631085 1.630434 -1.174020 H -0.758060 0.216776 -1.841134 H -2.551561 0.197706 -1.775959 H -0.733227 -0.108284 2.073539 H -0.868474 1.510861 1.320368 H 1.510679 0.219691 1.559161 H 1.365899 2.433188 0.472913 H 0.804891 1.698804 -1.040351 H 2.419810 1.348845 -0.433967 H 2.362284 -1.969077 -0.128218	71.5807 89.1262 106.0388 182.2582 192.8988 231.8138 241.6249 276.4663 300.0958 361.3803 374.6168 452.7035 491.1547 600.9474 670.5680 828.8478 874.1941 919.5503 945.0815 995.5859 1024.7476 1069.9956 1082.4532 1108.4310 1149.2068 1214.8025 1276.9284 1320.2746 1335.4639 1381.9608 1421.3115 1434.3200 1443.7610 1451.0193 1463.0212 1484.8736 1504.4664 1647.0719 3053.6306 3070.5252 3087.3099 3093.7713 3163.3239 3165.4910 3174.7026 3184.6296 3210.5439 3808.7044

V. Simulation of Vibronic Envelopes:

The vibrationally-resolved photoionization spectra were simulated using a locally modified version of Gaussian. To set up the computational protocol, calculations were first performed at T=0K using the sum-over-states (time-independent, TI) formulation[16] where the spectrum is obtained as an ensemble of distinct transitions between the vibrational initial and final states, within both adiabatic Hessian (AH) and vertical Hessian (VH) methods to describe the final-state potential energy surface. In AH, the harmonic potential energy surface is computed about the final-state minimum, while for VH, the surface is computed at the initial-state minimum. If there are no structural changes upon ionization, the spectra computed with AH or VH will give the same results. Otherwise, they generally represent limit conditions, with VH predicting better band intensities, while AH predict better their positions. It should be noted that, since the final-state equilibrium structure is unknown with VH, it is extrapolated assuming that the potential energy surface is purely harmonic. While this can sometimes lead to better results thanks to an error compensation due to the harmonic approximation assumed to compute the spectral band-shape, it can also lead to severe misrepresentations of the structural changes. This is discussed in more details below.

As with our previous work on tert-butyl hydroperoxide,[17] the structural changes for most conformers are quite large with strong mode mixing. It is noteworthy that the use of the AH or VH models leads to very different behaviors. For AH, Cartesian-based normal coordinates are clearly ill-

suited, with the predicted spectra being extremely broad and with very weak intensities. The use of *ad hoc* internal coordinates, more specifically the generalized internal coordinates (see Baiardi et al.[18] for details), is necessary to predict correctly the band-shapes or, for some conformers, even get any result. To reach a good convergence, that is, being able to recover all non-negligible transitions within the TI framework, a reduced-dimensionality scheme had to be applied. For Cartesian coordinates, the number of modes to remove was excessively large (up to 40 out of 48), rendering the result unusable. For internal coordinates, the modes to be removed were first selected based on the shift vector from the Duschinsky transformation[19] (*K*), considering modes from the initial states shifted by at least 0.75 atomic units. Then, modes from the final and initial states to discard were chosen iteratively based on their overlap using the Duschinsky matrix. The threshold for the convergence was set to 0.7 (0.65 for conf-4) using the algorithm described in section F of Baiardi et al.[18]. For the three most abundant conformers, 8 modes were removed: 1, 2, 4-6, 11-13 for the initial state of conf-1, ordering the modes by increasing energy, 1-4, 7- 10 for conf-2, and 1-8 for conf-4 within the AH model. The final progression, using the class-based prescreening described in Santoro et al.[20] with parameters C_1^{max}=50, C_2^{max}=50, and N_I^{max}=10^9, was 96.54% for conf-1, 98.59% for conf-2 and 94.54% for conf-4. For VH, because of the lower predicted shift, a threshold of 0.8 was sufficient to construct the blocks of modes to remove. Using the same base criterion to select the initial group of modes to remove, 6 modes were removed for conf-1 (1- 4, 12, 13), 4 for conf-2 (1-4) and 5 for conf-4 (1, 2, 4-6). The progression reached almost 100%, respectively at 99.66%, 99.87% and 99.97%.

For VH, the differences between internal and Cartesian coordinates are more subtle. First of all, the cations of conformers 1, 2 and 4 exhibited one or two imaginary frequencies at the neutral-form equilibrium geometry. They were systematically selected to be removed. Initial-state modes with an associated shift (K_i) greater than 75 atomic units were also selected. As a result, and choosing a threshold of 0.8 to build a consistent set of modes to remove in each states, 6 modes were selected for conf-1 (1-4, 12, 13 in the initial state), 3 modes for conf-2 (1-3) and 6 for conf-4 (1-6). The total progression was respectively 99.90%, 99.44% and 99.97%.

The final spectra are shown in Fig. S5. Gaussian distribution functions with half-widths at half maximum of 250 cm^{-1} were used to match experiment.

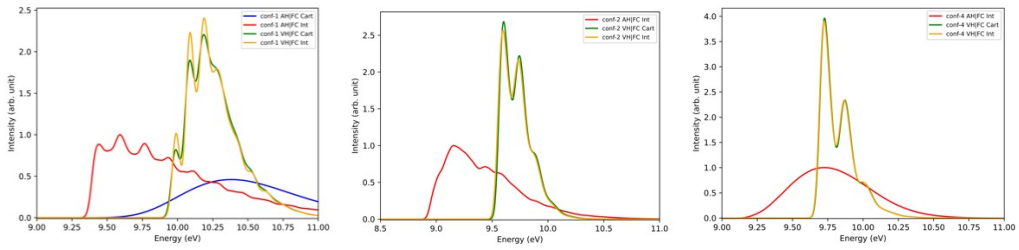

Figure S5. Simulated PES of conformers 1 (left), 2 (center) and 4 (right) of 2,4-KHP at the TI AH|FC and VH|FC levels at T=0 K. Gaussian distribution functions with half-widths at half-maximum of 250 cm^{-1} were used to simulate the experimental broadening. To compare internal and Cartesian AH|FC band-shapes, the modes automatically selected with internal coordinates were used for Cartesians and mode mixing was ignored to have model systems of the same size. For conformers 2 and 4, it was impossible to get any band-shape.

The excellent progression obtained with the reduced-dimensionality schemes confirm the applicability of the Franck-Condon principle in these conditions. To ensure that fully converged band-shapes were systematically obtained and to include temperature effects in a cost-effective manner, the time-dependent (TD) framework described in Baiardi et al.[21] was then used for an implicit inclusion of all possible transitions by exploiting the properties of the Fourier transform. The default parameters reported in the original paper were used to compute the auto-correlation function and build the resulting spectrum.

Proceeding further into our analysis, since augmented basis functions can play a greater role in the calculation of normal modes and frequencies than for the structure, the harmonic PES of the neutral and cationic forms of the three most abundant conformers were computed at the M06-2X-D3/aug-cc-pVTZ as well. As shown in Fig. S6, the changes are practically negligible in the spectral band-shapes. The normal modes are only slightly different, and all wavenumbers within 10 cm^{-1}. As a result, and for consistency with the rest of the analysis, only the cc-pVTZ results were used.

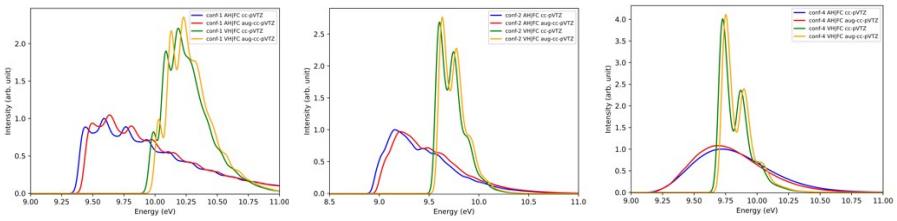

Figure S6. Comparison of the simulated PES of conformers 1 (left), 2 (center) and 4 (right) of 2,4-KHP at the TD AH|FC and VH|FC levels at T=0K. The potential energy surfaces were computed at the M06-2X-D3/cc-pVTZ and the M06-2X-D3/aug-cc-pVTZ. Gaussian distribution functions with half-widths at half-maximum of 250 cm^{-1} were used to simulate the experimental broadening.

To further analyze the sensitivity of the spectra to the uncertainties in the relative energies, we performed simulations at three different temperatures: 300 K, 585 K, and 800 K (Figure S7). At lower temperatures (300 K), the most stable conformer (conformer 1) dominates. The lower temperature also leads to less broadening caused by hotbands, resulting in sharper spectral features. At higher temperatures (585 K and 800 K), the populations become more evenly distributed among the conformers and mostly stabilized. The contributions from more populated initial vibrational states

lead to broader spectral features. Despite these changes in populations, the overall spectral trends remain relatively consistent across temperatures, highlighting the robustness of the simulated spectra with respect to uncertainties in the relative free energies of the conformers.

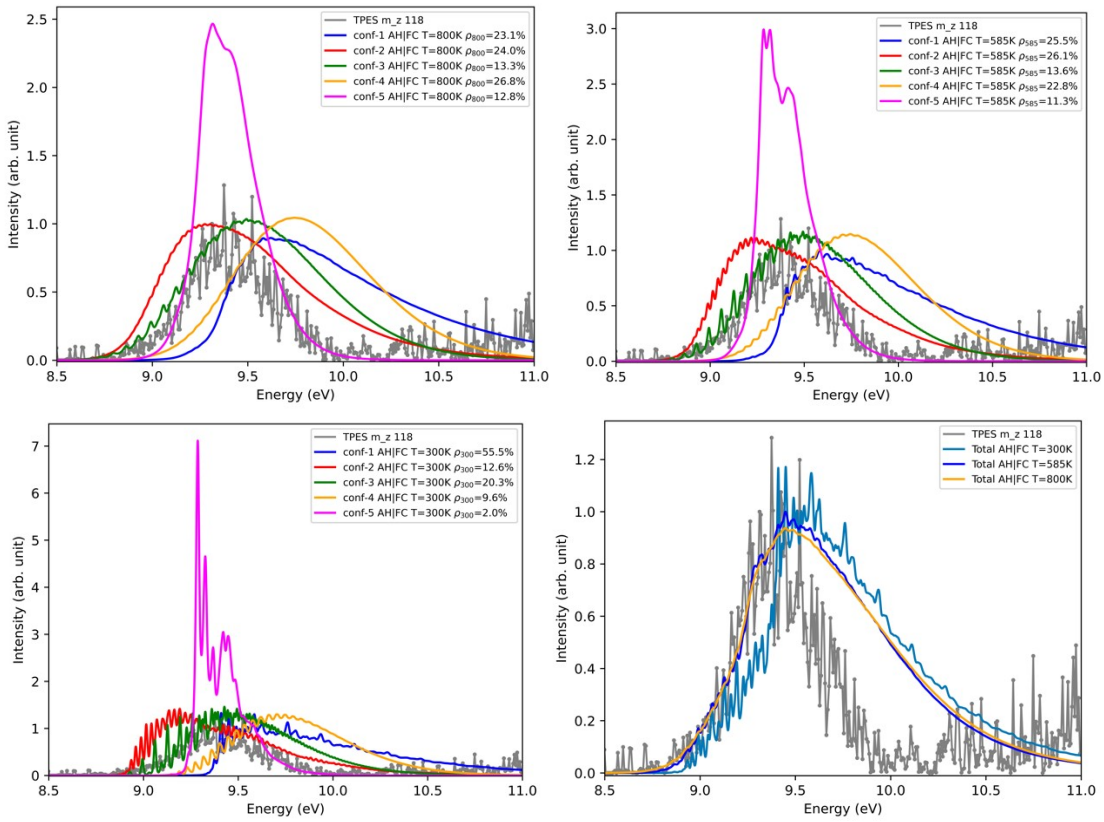

Figure S7. Simulated spectra at three different temperatures (300 K, 585 K, and 800 K) and their impact on conformer populations and overall spectral shapes.

As a final analysis, we compared the structural changes predicted by VH with the real minima (Fig. S7), the Duschinsky matrix with AH and VH (Fig. S8) and the shift vector (Fig. S9). From Fig. S7, the extrapolated minimum geometries from VH are systematically close to the initial-states ones, and relatively far from the real one, which means that VH strongly underestimates the structural changes. This is confirmed by the shift vectors, on overall slightly smaller than with AH. Together with a smaller mode mixing (Fig. S8), this explains the narrower band-shape obtained with VH, as shown in Fig. S10. The final spectra obtained by combining the contributions from the 5 most abundant conformers with their abundances calculated at T= 585 K are shown in Fig. S11. VH shows a significantly shifted and slightly narrower band-shape compared to experiment. Conversely, AH is in very good agreement in terms of band positions but slightly overestimates is width, as discussed in the main text.

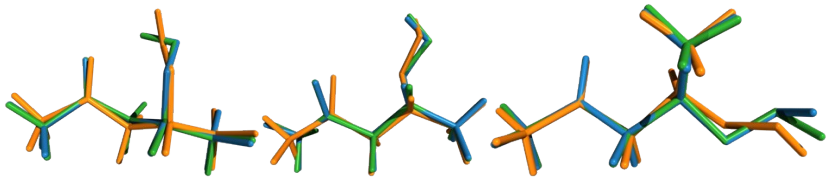

Figure S7. Comparison of initial-state equilibrium geometry (blue), final-state equilibrium geometry (orange), and extrapolated equilibrium geometry within the VH model (green) for conformers 1 (left), 2 (center) and 4 (right) 2,4-KHP. The structures were superimposed to minimize the rotations and translations between the structures.

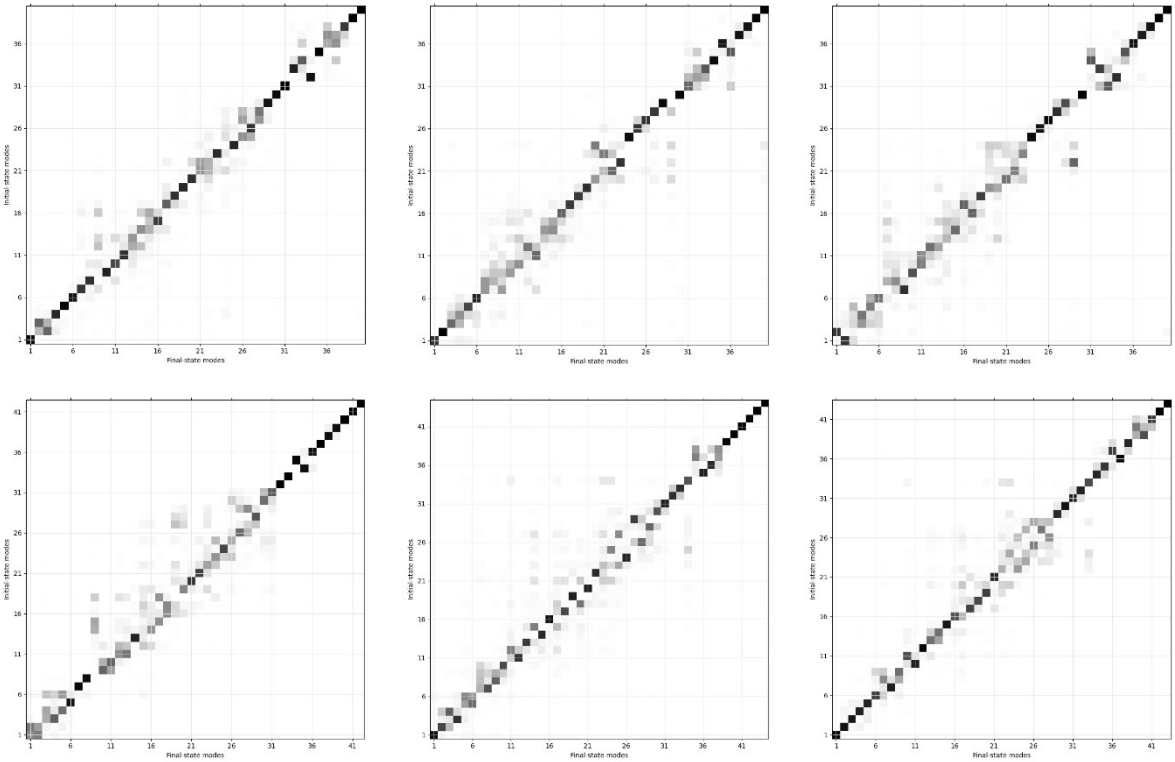

Figure S8. Comparison of the graphical representations of the Duschinsky matrices J at the AH (top) and VH (bottom levels) of conformers 1 (left), 2 (center) and 4 (right) 2,4-KHP, with normal modes based on internal coordinates. The squared value of each element was computed and divided by the sum of all elements in each row, then a shade of gray from white (0) to black (1) was assigned in the matrix.

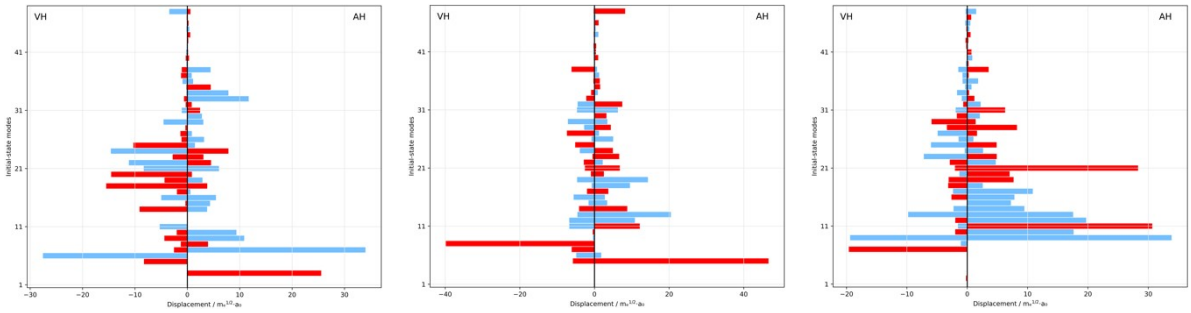

Figure S9. Comparison of the graphical representations of the shift vector K from the Duschinsky transformation conformers 1 (left), 2 (center) and 4 (right) 2,4-KHP. To show the magnitudes of the

displacements, absolute values are reported, and negatives values are showed in red. The absolute values are multiplied by -1 for the VH shift vector. To facilitate comparisons, all modes are shown. A null value was assigned to each mode removed from the reduced-size model.

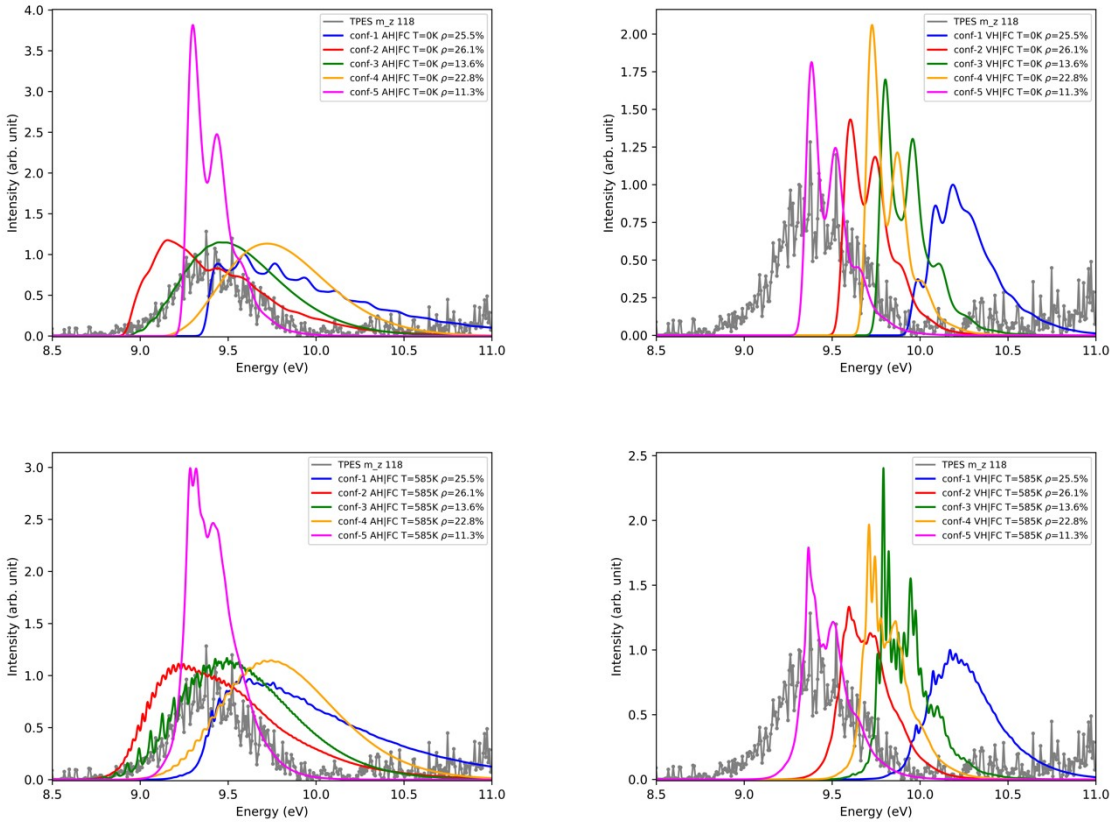

Figure S10. Comparison of the simulated PES of the 5 most abundant conformers of 2,4-KHP at the TD AH|FC (left) and VH|FC (right) at T=0 K (top) and 585 K (bottom). Gaussian distribution functions with half-widths at half-maximum of 250 cm^{-1} were used to simulate the experimental broadening at T=0 K and 50 cm^{-1} at T=585 K. The intensities were normalized based on the total intensity, assuming a Boltzmann population (ρ) of 1 for each conformer. The computed abundances are reported in the legend.

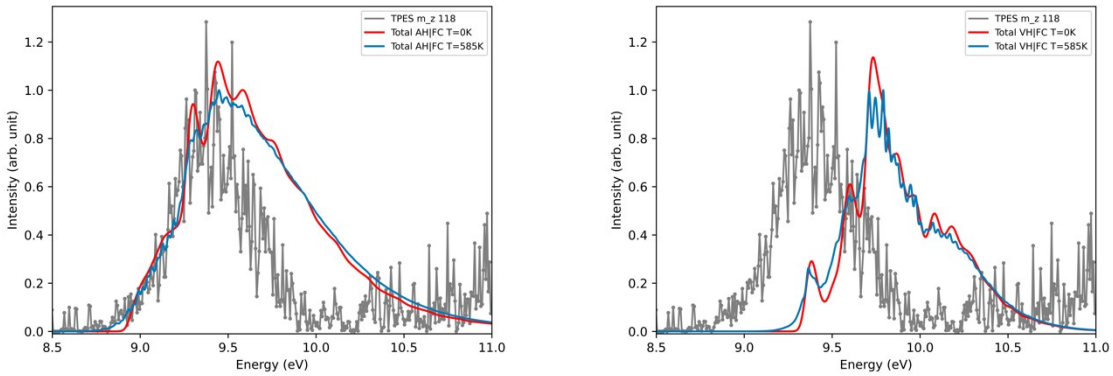

Figure S11. Comparison of the simulated PES of 2,4-KHP including the 5 most abundant conformers at the TD AH|FC (left) and VH|FC (right) levels. Gaussian distribution functions with half-widths at half-maximum of 250 cm^{-1} were used to simulate the experimental broadening at T=0 K and 50 cm^{-1} at T=585 K.

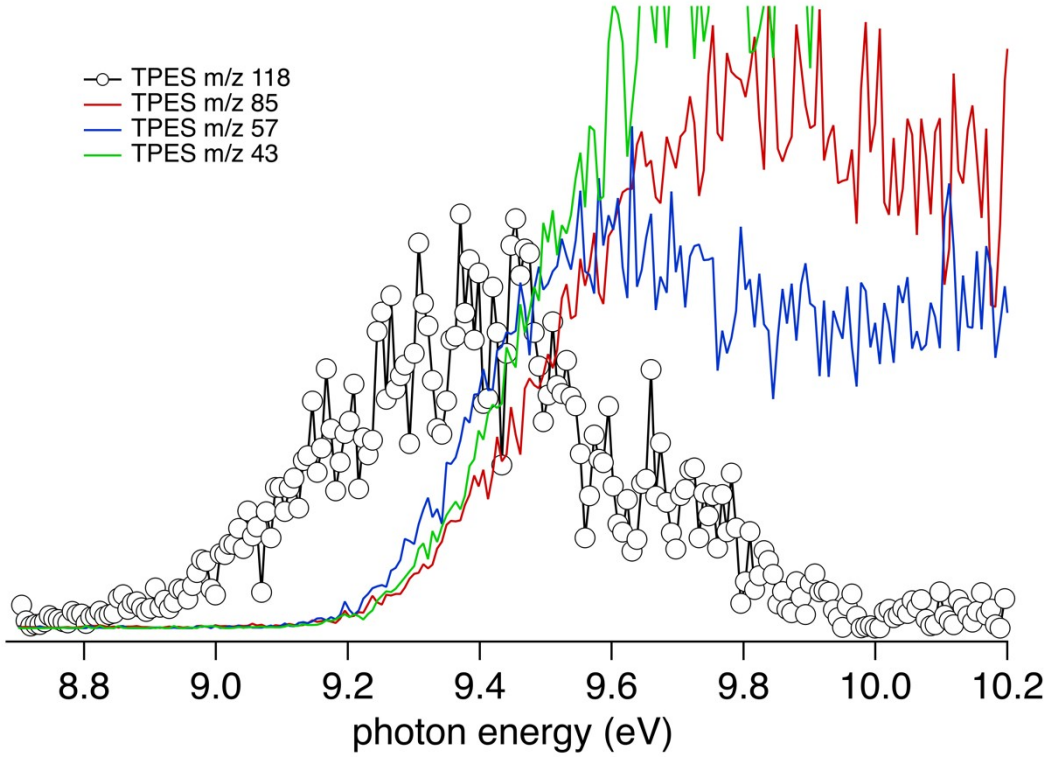

Figure S12.TPES of m/z 43 (green line), 57 (blue line), 85 (red line), and 118 (open dots) from Battin-Leclerc et al.[22]

VI. KHP Quantification Method:

Quantification of KHP was achieved via several ways. Similar to the method employed in Bourgalais et al.[23], an internal standard with a known mole fraction was used at 10.5 eV to convert the normalized ion signal of a given species to its mole fraction. At 10.5 eV, the mole fraction of reaction products can be calculated with the fuel, *n*-pentane, as a reference:

$$x_i(T) = x_{fuel}(T) \cdot \frac{S_i(T,E)}{S_{fuel}(T,E)} \cdot \frac{\sigma_{fuel}(E)}{\sigma_i(E)} \cdot \frac{D_{fuel}}{D_i}$$

$x_i(T)$, $S_i(T,E)$, and $\sigma_i(E)$ represent respectively the mole fraction, the signal, and the PICS of species *i* at the photon energy *E* and the temperature *T*. D_i is the mass discrimination factor of species *i* approximated as the square root of the mass of each species *i*. For the quantification of KHP, there are three different ways of determining the molar fraction:

(1) by using the parent signal of KHP at m/z 118 and its partial experimental PICS from Hu et al.[2] (1.13 Mb at 10.6 eV).

(2) by using the signal of each KHP fragment and its partial experimental PICS (from Hu et al.[2], m/z 85 fragment has a partial PICS of 7.36 Mb at 10.6 eV).

(3) by using the total signal of KHP (parent m/z 118 + fragments: m/z 43, 57, and 85) and the corresponding total PICS estimated using Bobeldijk's method[24] based on bond additivity: 21.25 Mb at 10.6 eV with an uncertainty of ~25% based on values provided by Rodriguez et al.[25] The details of the calculation are provided below:

$$\sigma_{C5H10O3} = (4 \times \sigma_{C-C}) + (1 \times \sigma_{C-O}) + (1 \times \sigma_{C=O}) = (4 \times 2.03) + (1 \times 4.83) + (1$$

It should be noted that in this estimation of the cross section, it is assumed that the contribution of the O-O group is zero, which may potentially underestimate the cross section.

The total uncertainty propagation is:

$$\Delta R = \sqrt{(0.64 \times 8.12)^2 + (0.16 \times 4.83)^2 + (0.12 \times 8.30)^2} = 5.35\ Mb$$

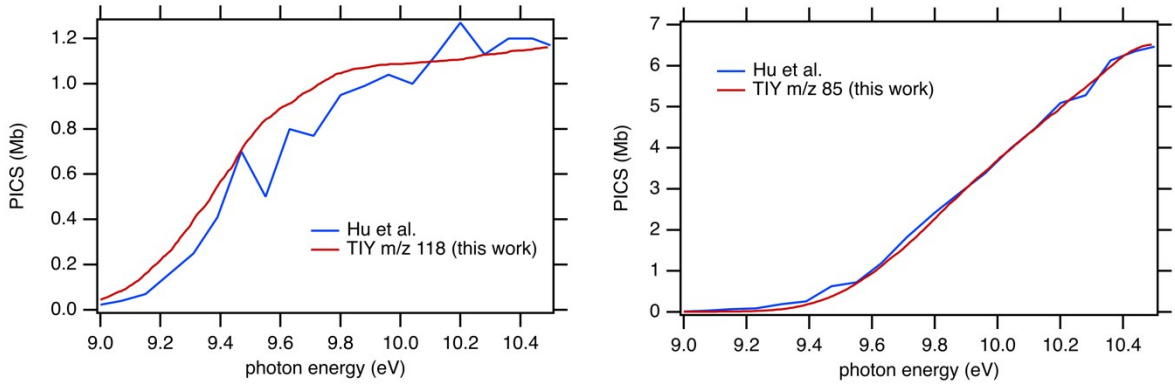

Figure S13. Comparison between the TIY of m/z 118 (left panel) and m/z 85 (right panel) registered in this work (red line) and in Hu et al.[2] (blue line).

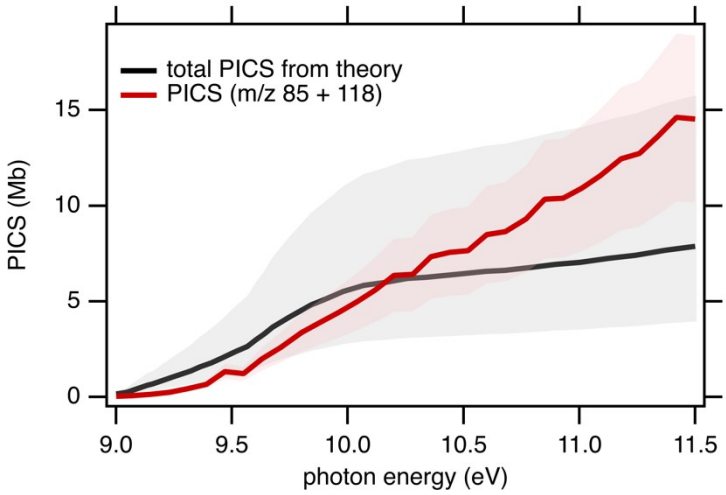

Figure S14. Comparison between the sum of the PICS m/z 85 and 118 from Hu et al.[2] (red line) and the total PICS calculated using the method by Moshammer et al.[26] (black line).

References:

1 D. L. Osborn, P. Zou, H. Johnsen, C. C. Hayden, C. A. Taatjes, V. D. Knyazev, S. W. North, D. S. Peterka, M. Ahmed and S. R. Leone, *Review of Scientific Instruments*.

2 Z. Hu, Q. Di, B. Liu, Y. Li, Y. He, Q. Zhu, Q. Xu, P. Dagaut, N. Hansen, S. M. Sarathy, L. Xing, D. G. Truhlar and Z. Wang, *Proc. Natl. Acad. Sci. U.S.A.*, 2023, 120, e2220131120.

3 F. Jorand, A. Heiss, O. Perrin, K. Sahetchian, L. Kerhoas and J. Einhorn, *International journal of chemical kinetics*, 2003, 35, 354–366.

4 M. Bursch, J.-M. Mewes, A. Hansen and S. Grimme, *Angewandte Chemie International Edition*, 2022, 61, e202205735.

5 T. Lu, Molclus program, version 1.12, http://www.keinsci.com/research/molclus.html.

6 C. Bannwarth, S. Ehlert and S. Grimme, *J. Chem. Theory Comput.*, 2019, 15, 1652–1671.

7 S. Grimme, C. Bannwarth and P. Shushkov, *J. Chem. Theory Comput.*, 2017, 13, 1989–2009.

8 Y. Zhao and D. G. Truhlar, *Theor Chem Account*, 2008, 120, 215–241.

9 S. Grimme, J. Antony, S. Ehrlich and H. Krieg, *J. Chem. Phys.*, 2010, 132, 154104.

10 T. H. Dunning, *J. Chem. Phys.*, 1989, 90, 1007–1023.

11 K. Raghavachari, G. W. Trucks, J. A. Pople and M. Head-Gordon, *Chemical Physics Letters*, 1989, 157, 479–483.

12 T. Lu and Q. Chen, *Computational and Theoretical Chemistry*, 2021, 1200, 113249.

13 I. M. Alecu, J. Zheng, Y. Zhao and D. G. Truhlar, *J. Chem. Theory Comput.*, 2010, 6, 2872–2887.

14 M. J. Frisch, G. W. Trucks, H. B. Schlegel, G. E. Scuseria, M. A. Robb, J. R. Cheeseman, G. Scalmani, V. Barone, G. A. Petersson, H. Nakatsuji, X. Li, M. Caricato, A. V. Marenich, J. Bloino, B. G. Janesko, R. Gomperts, B. Mennucci, H. P. Hratchian, J. V. Ortiz, A. F. Izmaylov, J. L. Sonnenberg, Williams, F. Ding, F. Lipparini, F. Egidi, J. Goings, B. Peng, A. Petrone, T. Henderson, D. Ranasinghe, V. G. Zakrzewski, J. Gao, N. Rega, G. Zheng, W. Liang, M. Hada, M. Ehara, K. Toyota, R. Fukuda, J. Hasegawa, M. Ishida, T. Nakajima, Y. Honda, O. Kitao, H. Nakai, T. Vreven, K. Throssell, J. A. Montgomery Jr., J. E. Peralta, F. Ogliaro, M. J. Bearpark, J. J. Heyd, E. N. Brothers, K. N. Kudin, V. N. Staroverov, T. A. Keith, R. Kobayashi, J. Normand, K. Raghavachari, A. P. Rendell, J. C. Burant, S. S. Iyengar, J. Tomasi, M. Cossi, J. M. Millam, M. Klene, C. Adamo, R. Cammi, J. W. Ochterski, R. L. Martin, K. Morokuma, O. Farkas, J. B. Foresman and D. J. Fox, Gaussian 16 Rev. C.01 2016.

15 F. Neese, *WIREs Comput Mol Sci*, 2018, 8, e1327.

16 M. Biczysko, J. Bloino, F. Santoro and V. Barone, in *Computational Strategies for Spectroscopy*, John Wiley & Sons, Ltd, 2011, pp. 361–443.

17 J. Bourgalais, Z. Jiang, J. Bloino, O. Herbinet, H.-H. Carstensen, G. A. Garcia, P. Arnoux, L.-S. Tran, G. Vanhove, L. Nahon, F. Battin-Leclerc and M. Hochlaf, *Phys. Chem. Chem. Phys.*, 2022, 24, 10826.
18 A. Baiardi, J. Bloino and V. Barone, *J. Chem. Phys.*, 2016, 144, 084114.
19 F. Duschinsky, *Acta Physicochim. URSS*, 1937, 7, 551–566.
20 F. Santoro, R. Improta, A. Lami, J. Bloino and V. Barone, *J. Chem. Phys.*, 2007, 126, 084509.
21 A. Baiardi, J. Bloino and V. Barone, *J. Chem. Theory Comput.*, 2013, 9, 4097–4115.
22 F. Battin-Leclerc, J. Bourgalais, Z. Gouid, O. Herbinet, G. Garcia, P. Arnoux, Z. Wang, L.-S. Tran, G. Vanhove and L. Nahon, *Proceedings of the Combustion Institute*, 2021, 38, 309–319.
23 J. Bourgalais, O. Herbinet, H.-H. Carstensen, J. Debleza, G. A. Garcia, P. Arnoux, L. S. Tran, G. Vanhove, B. Liu, Z. Wang, M. Hochlaf, L. Nahon and F. Battin-Leclerc, *Energy Fuels*, 2021, 35, 19689–19704.
24 M. Bobeldijk, W. J. van der Zande and P. G. Kistemaker, *Chemical Physics*, 1994, 179, 125–130.
25 A. Rodriguez, O. Herbinet, X. Meng, C. Fittschen, Z. Wang, L. Xing, L. Zhang and F. Battin-Leclerc, *J. Phys. Chem. A*, 2017, 121, 1861–1876.
26 K. Moshammer, A. W. Jasper, D. M. Popolan-Vaida, Z. Wang, V. S. Bhavani Shankar, L. Ruwe, C. A. Taatjes, P. Dagaut and N. Hansen, *J. Phys. Chem. A*, 2016, 120, 7890–7901.